

## A seafloor long-baseline tiltmeter

Gregory Anderson, Steven Constable, Hubert Staudigel, and Frank K. Wyatt

Institute of Geophysics and Planetary Physics, Scripps Institution of Oceanography, University of California, San Diego

**Abstract.** Long-term monitoring of seismicity and deformation has provided constraints on the eruptive behavior and internal structure and dynamics of subaerial volcanoes, but until recently, such monitoring of submarine volcanoes has not been feasible. Little is known about the formation of oceanic crust or seamounts, and we have therefore developed a stand-alone long-baseline tiltmeter to record deformation on active seafloor volcanoes. The instrument is a differential pressure, two-fluid sensor adapted for use on the seafloor, combined with an autonomous data logger and acoustic navigation/release system. The tiltmeter can be installed without use of remotely operated vehicles or manned submersibles and, to first order, is insensitive to noise driven by temperature or pressure gradients. We recorded 65 days of continuous data from one of these tiltmeters on Axial Seamount on the Juan de Fuca Ridge during a multidisciplinary experiment that included ocean bottom seismographs, magnetotelluric instruments, and short-baseline tiltmeters. After instrument equilibration the 100-m-long tiltmeter provided a record with long-term drift rates of  $0.5\text{--}5\ \mu\text{rad day}^{-1}$  and higher frequency variations of the order of  $5\text{--}10\ \mu\text{rad}$ . Comparison with records of subaerial volcanic tilt shows that this instrument can discriminate volcanic deflation events, though none occurred during our deployment, a conclusion supported by nearby short-baseline tilt and bottom pressure recordings. The short- and long-baseline data constrain volcanic inflation of Axial Seamount to be below  $0.5\text{--}1\ \mu\text{rad day}^{-1}$  during mid-1994. Analysis of the long-baseline tilt data in conjunction with electric field, temperature, and short-baseline tiltmeter data shows that high-frequency signals are largely driven by ocean currents. Improved coupling between the tiltmeter and seafloor should reduce this noise, improve stability and drift, and further enhance our ability to record tilt related to active submarine volcanism.

### Introduction

Monitoring of subaerial volcanoes relies heavily on two complementary techniques: seismology and surface deformation. Each of these has its own distinct strengths, and the success of volcano monitoring decreases significantly if either technique is used in isolation. Seismology is unmatched in early detection of intrusive activity and accuracy in locating brittle deformation events. During volcanic crises, harmonic tremor is crucial for pinpointing major magma flow. However, magma flow itself does not cause earthquakes, and other techniques must be used to detect aseismic magma redistribution within a volcano. Surface deformation measurements are unique in providing constraints on the temporal evolution of melt accumula-

tion, the behavior of magma redistribution through volcanic feeder systems, and the fraction of available melt that has been erupted at the surface versus emplaced in shallow dike systems. Continuous surface deformation measurements, however, are limited in their ability to pinpoint the location of intrusions or the force of magmatic injection because of the small size of the signals, the existence of environmental noise, and the difficulty of uniquely inferring the source of the signal. Thus complementary monitoring techniques and verification of measurements through redundancy are key in volcano monitoring.

Use of such combined techniques on major subaerial volcanoes has provided key details on the geometry of magma feeder systems, temporal and spatial behavior of

magma influx from depth into shallow reservoirs, redistribution of melt within a volcano, and eruptive behavior of volcanoes [e.g., Klein, 1984; Decker, 1987; Klein et al., 1987]. These techniques have thus been extremely successful in improving our understanding of how volcanic systems work and in predicting the timing and types of eruptions, but all major advances in this field have come from studies on a few very well-instrumented volcanoes [Decker, 1987]. Until recently, technical difficulties have precluded meaningful long-term monitoring of the most abundant types of volcanoes exposed in the submarine environment, so there is much still to be learned about how ocean crust or seamounts are formed.

Significant effort has been expended to fill this gap in our understanding of volcanoes, focusing on seismology and surface deformation. Marine seismology has long been an established discipline [e.g., Bradner et al., 1965; Johnson et al., 1977; Willoughby et al., 1993], but the development of seafloor deformation measurements has begun only recently [e.g., Staudigel et al., 1990; Chadwell et al., 1995; Wyatt et al., 1996]. In this paper we shall discuss the development of a seafloor long-baseline tiltmeter, including the results of a successful test deployment at the Juan de Fuca Ridge.

## Tiltmeters for Submarine Volcano Monitoring

Surface deformation can be measured in many different ways, including tilt, strain, and geodetic techniques; of these, tilt is used most frequently for volcano monitoring. The Westphal short-baseline instrument [Westphal et al., 1983] is the most commonly used tiltmeter, but long-baseline designs have also played a major role at some subaerial observatories [e.g., Wyatt et al., 1984; Davis et al., 1987]. Short-baseline tiltmeters (SBTs), that is, with baseline of the order of  $\leq 1$  m, have the main advantage of being relatively inexpensive and easy to install. However, SBTs are sensitive primarily to short-wavelength tilt and noise, which we expect to be highly heterogeneous in fragmented volcanic environments. Also, SBTs are subject to creep instability in the instrument itself and can be strongly influenced by very localized fluctuations in temperature, rain, and other such effects.

Long-baseline tiltmeters (LBTs), with baseline of the order of  $\geq 10$  m, have several potential advantages over the SBT design. By virtue of their greater baseline length they are less sensitive to short-wavelength noise masking the broader-scale deformation field. They are also inherently much less susceptible than SBTs to the effects of creep instability in the instrument components or ground coupling. However, LBTs typically are more expensive and much more difficult to install than SBTs and are susceptible to different sources of noise.

Seafloor environmental conditions present both major advantages over subaerial conditions and serious challenges to the successful use of tiltmeters for submarine volcanic monitoring. The primary advantage of the seafloor is that environmental conditions such as temperature are much more stable than those on land; for example, typical seafloor diurnal temperature fluctuations are  $\pm 0.1^\circ\text{C}$  in comparison with about  $\pm 15^\circ\text{C}$  experienced by the LBT on land at Piñon Flat Geophysical Observatory [Wyatt and Berger, 1980]. However, while fluctuations in these conditions are low, the average conditions themselves are extreme. Cold temperatures (near  $0^\circ\text{C}$ ) and high confining pressures (1 MPa per 100 m depth) can cause creep of instrument parts, contact with seawater will cause corrosion if care is not taken in selecting materials for use in a seafloor tiltmeter, and coupling instabilities can result in noise driven by seafloor currents. Furthermore, the condition of a candidate site on the seafloor is barely known in comparison with a subaerial site, and it is often impossible to determine before deployment whether or not a particular area is primarily mud, rubble, or relatively stable bedrock. For these and other reasons it is quite difficult to achieve the same level of performance with a seafloor instrument as with subaerial instruments.

Is it feasible to build a tiltmeter capable of recording geophysically relevant signals on the seafloor given the extreme conditions there? Tilt driven by relative plate motion on continents typically shows rates of  $0.1\text{--}0.3 \mu\text{rad yr}^{-1}$  [Wyatt et al., 1988], well below the minimum tilt rates that can be detected by current seafloor tiltmeters. However, tilt driven by eruptive or intrusive volcanic events can have much higher rates [e.g., Dvorak et al., 1986], which may be within the reach of current technology. Simple models of volcanic deflation provide bounds on tilt rates that might be observed during a volcanic event.

Eruptions of Kilauea Volcano on Hawaii give some constraints on the rates and volumes of magma injection during intrusive events at a hotspot volcano. Injection rates during Kilauean volcanic crises are often greater than  $10^6 \text{ m}^3 \text{ day}^{-1}$  and can be as much as  $10^8 \text{ m}^3 \text{ day}^{-1}$  [e.g., Pollard et al., 1983; Dvorak et al., 1986]. When we compute the surface displacements and tilts produced by deflating a 2-km-radius Mogi source [Mogi, 1958] centered 5 km below the surface at rates of  $10^6$ ,  $10^7$ , and  $10^8 \text{ m}^3 \text{ day}^{-1}$ , we find tilt rates of about 1, 10, and  $100 \mu\text{rad day}^{-1}$  over a distance of 2–10 km from the volcano (Figure 1a).

Measurements of dike dimensions in ophiolites [e.g., Baragar et al., 1987; Rothery, 1983] and data from eruptions on Iceland [e.g., Sigurdsson, 1987] and along the CoAxial segment of the Juan de Fuca Ridge [Dziak et al., 1995] can be combined to estimate magma injection rates that might occur during dike formation along an active segment of the mid-ocean ridge (MOR);

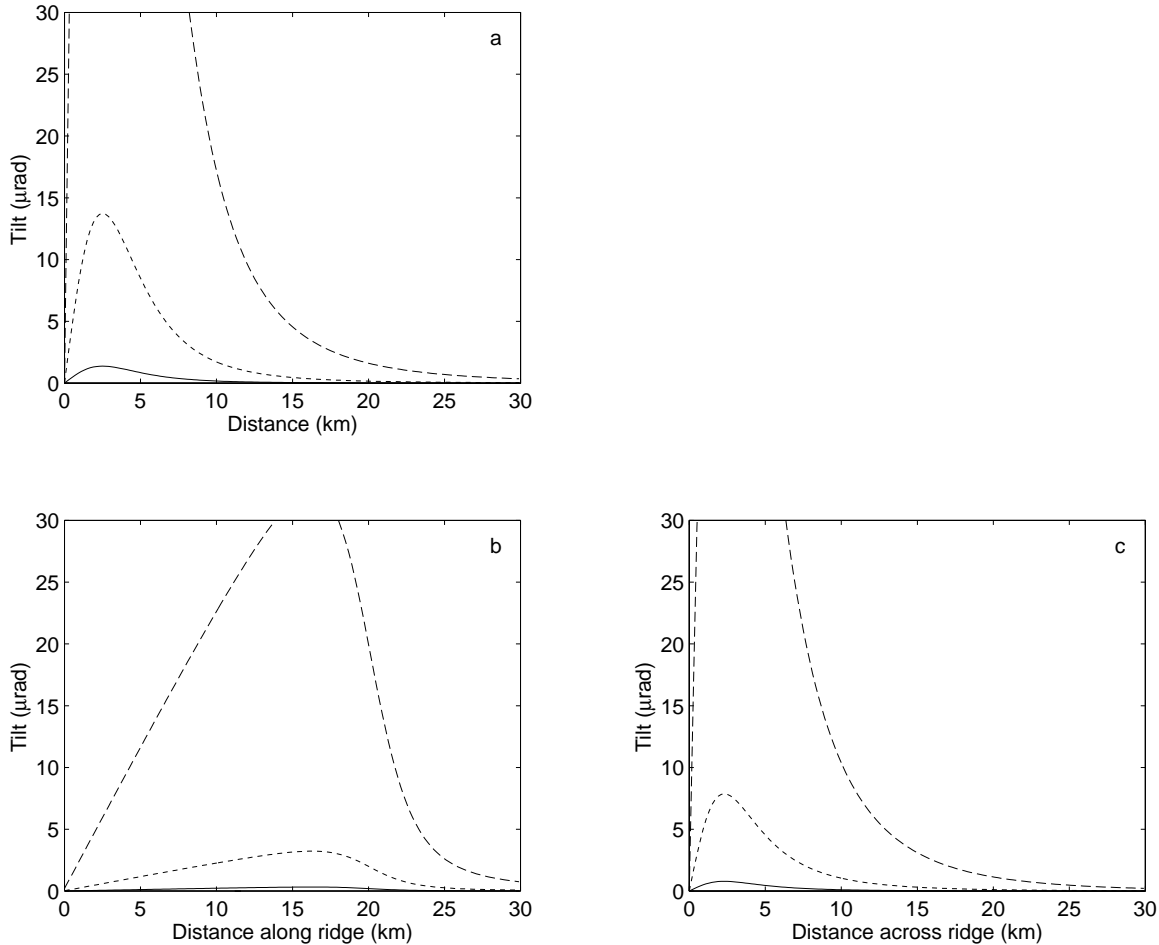


**Figure 1.** (a) Estimated tilt for models of a deflating Mogi source 2 km in radius, centered 5 km below the surface in an elastic half-space with Lamé constants  $\lambda = \mu = 30$  GPa. Solid curve is tilt rate that would result from removing  $10^6 \text{ m}^3 \text{ day}^{-1}$  of magma from the source, the short-dashed curve is for  $10^7 \text{ m}^3 \text{ day}^{-1}$ , and the long-dashed line is for  $10^8 \text{ m}^3 \text{ day}^{-1}$ . (b) Estimated along-ridge tilt for models of a deflating Yang source with a semimajor axis of 20 km, a semiminor axis of 2 km, and a centroid depth of 4 km. Curve notation as in Figure 1a. (c) Estimated across-ridge tilt for the same Yang source as in Figure 1b. Curve notation as in Figures 1a and 1b.

a reasonable range is  $10^6$ – $10^8 \text{ m}^3 \text{ day}^{-1}$ . On the basis of the axial magma chamber (AMC) observations of *Sinha et al.* [1997] we model an AMC along a segment of the MOR as a prolate spheroid with a 20-km semimajor axis, a 2-km semiminor axis, and a 4-km centroid depth. We then use the method of *Yang et al.* [1988] to compute the surface displacements and tilts produced by deflating our model AMC at rates of  $10^6$ ,  $10^7$ , and  $10^8 \text{ m}^3 \text{ day}^{-1}$  and find tilt rates of about 1, 10, and  $100 \mu\text{rad day}^{-1}$  over a distance of 2–10 km from the ridge axis across strike and about 0.5, 5, and  $50 \mu\text{rad day}^{-1}$  over a distance of 10–20 km along strike from the center of the AMC (Figures 1b and 1c).

We do not wish to imply that a particular volcano or ridge segment would behave as shown, but merely

that these models give a reasonable order-of-magnitude bound on tilt rates that might be observed in situ. It is also important to remember that such intrusive events might occur only episodically on an annual to decadal scale on any given seamount or MOR segment. Given these caveats, however, it is clear that tilt rates during volcanic crises are 3–5 orders of magnitude higher than tilt rates related to relative plate motions on continents. Thus, however unlikely it is that seafloor tiltmeters can be constructed to make meaningful measurements of slow tectonic tilt, constructing instruments with performance good enough to make them useful for our understanding of submarine volcanoes is a much more tractable problem.

## A Seafloor Long-Baseline Tiltmeter

Most of the techniques used in installing high-quality land instruments [Agnew, 1986] either cannot be applied to, or are prohibitively expensive in, the seafloor environment. For example, even installing a level instrument, a requirement for nearly all of the better tiltmeter designs, is extremely difficult without the use of remotely operated vehicles or manned submersibles, and free fluid surfaces, such as those in highly accurate Michelson-Gale LBTs [Wyatt *et al.*, 1984], are impractical under seafloor conditions. However, LBT designs that measure the pressure in fluid-filled tubes [e.g., *Beavan and Bilham*, 1977; *Agnew*, 1986] are feasible on the seafloor, and this is the approach we have chosen to pursue. Our development work has resulted in the design illustrated in Figure 2. It is a center-pressure instrument folded back on itself, with a sensor that measures the differential pressure between two tubes (arms) filled with fluids of differing densities, which terminate with fluid reservoirs (pots) that are sealed by compliant membranes. This design has several advantages. First, because the fluid reservoirs open to environmental pressure are side by side, the potentially significant seafloor lateral pressure gradients need be neither compensated for nor measured. Also, we require only one pressure sensor, which makes for simplicity and reliability in both the design and deployment of the instrument. Additionally, with an appropriate choice of fluid properties this LBT design can be made temperature compensating to first order, as discussed below.

The confining pressure of the seafloor environment presents a significant challenge in measuring tilt with this type of instrument. If the relative heights of the fluid reservoirs and the pressure sensor change by  $\Delta h$ , the corresponding pressure change is

$$\Delta P = (\rho_1 - \rho_2)g\Delta h \quad (1)$$

where  $\rho_1$  and  $\rho_2$  are the fluid densities in the two tiltmeter arms. Our current instrument uses ethylene glycol and isopropanol; the density difference between these fluids under seafloor conditions is approximately  $1131 - 811 = 320 \text{ kg m}^{-3}$ . To measure a  $1\text{-}\mu\text{rad}$  tilt, corresponding to a relative elevation change of 0.1 mm over an instrument baseline of 100 m, we must therefore be able to measure differential pressure to better than 0.3 Pa. At a deployment depth of 1000-4000 m our instrument has to measure differential pressures while subjected to a common mode pressure  $10^7\text{--}10^8$  times larger. Also, since we intend the instrument to be useful on sloping terrain, we require an operating range sufficient to handle these slopes; our design currently has a dynamic range of about  $\pm 40 \text{ kPa}$ , which corresponds to 11 m height difference over a 100-m baseline. One commercial pressure sensor that fulfills our requirements is a variable reluctance gauge manufactured by Validyne (Validyne model DP215-36-N1S4A).

Although this transducer will tolerate large internal common mode pressures, we operate it in a pressure-compensated oil bath to avoid creep of the component materials, which would otherwise tend to introduce drift into the measurements.

### Thermal Noise

On land, thermal fluctuations are the largest sources of noise for tiltmeters, and although seafloor temperature variations are much lower, their effects are still important. *Beavan and Bilham* [1977] have detailed the effect of thermal noise on fluid tube tiltmeters; here we give only a brief review. If a fluid tube tiltmeter is perturbed by a change in temperature along its length,  $\Delta T(s)$ , there will be a corresponding pressure change given by

$$\begin{aligned} \Delta P[\Delta T(s)] &= K_1 \int_0^S \Delta T(s) \sin \theta(s) ds \\ &+ K_2 \int_0^S \Delta T(s) ds \\ &+ K_3 \int_0^Y \Delta T(y) dy \end{aligned} \quad (2)$$

where

$$K_1 = -(\rho_1\beta_1 - \rho_2\beta_2)g \quad (3)$$

$$K_2 = [\rho_1(\beta_1 - 3\beta_t) - \rho_2(\beta_2 - 3\beta_t)]\frac{A_t}{A_p}g \quad (4)$$

$$K_3 = -(\rho_1 - \rho_2)g\beta_p \quad (5)$$

and  $\rho_1$ ,  $\rho_2$ ,  $\beta_1$ , and  $\beta_2$  are the densities and thermal expansivities of the two fluids;  $A_t$ ,  $A_p$ ,  $\beta_t$ , and  $\beta_p$  are the cross-sectional areas and thermal expansivities of the tubing and fluid reservoirs respectively;  $S$  is the length of the tiltmeter;  $\theta(s)$  is the angle from the horizontal of the tube element  $ds$ ; and  $Y$  is the depth of fluid in the fluid reservoir. The first term in (2) is usually the largest, whereas the other terms are second-order effects related to thermal expansion of the tiltmeter tubing and fluid reservoirs, respectively. However, if the two fluids are chosen such that the product of density and thermal expansivity ( $\rho\beta$ ) is the same or nearly so for each arm, the first term in (2) is greatly reduced, and the entire instrument is temperature compensating.

Our seafloor instrument has arms 100 m long, made of 0.22-inch ID soft alloy copper tubing with 6-inch ID aluminum end reservoirs (a permanent observatory installation would use all stainless steel or titanium construction). One arm is filled with ethylene glycol, and the other is filled with isopropanol; see Table 1 for the relevant properties of these materials. By using (2) and assuming a 1-m height difference between the ends of the tiltmeter, each  $1^\circ\text{C}$  average temperature increase along the tiltmeter produces a pressure of  $-6.3403 + 0.7732 - 0.0251 = -5.5922 \text{ Pa}$  for

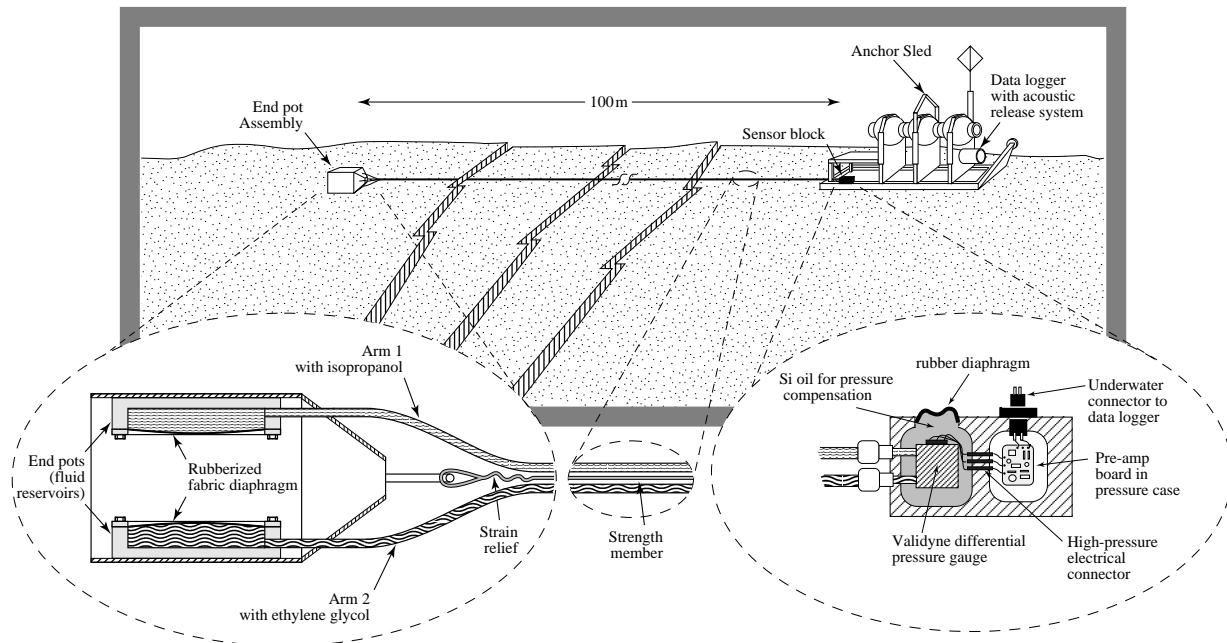


**Figure 2.** Conceptual diagram showing the design of our seafloor LBT.

the arm filled with ethylene glycol and a pressure of  $-6.4363 + 0.8085 - 0.0180 = -5.6458$  Pa for the isopropanol arm. The result is a temperature-driven differential pressure of only 0.0536 Pa, or, using (1),  $0.171 \mu\text{rad}$ . As expected, while the first term in (2) dominates for each fluid individually, the resultant differential pressure is quite small; thus the instrument should be temperature compensating to first order.

Since it is difficult to estimate the product  $\rho\beta$  accurately under seafloor conditions, we have also chosen to measure the quantity  $\int_0^S \Delta T(s) ds$ , the along-tiltmeter temperature, directly. A standard four-conductor, 28-gauge copper telephone cable runs along the tiltmeter with the conductors connected in series, giving a total length of 400 m. The resistance temperature coefficient of this length of cable is  $0.34 \Omega \text{ K}^{-1}$ ; we supply a constant current and measure the resulting voltage as our estimate of integrated temperature. Using this record, we can estimate the LBT temperature coefficient and use it to reduce the thermal noise in the final data.

## Deployment

Ideally, we would use remotely operated vehicles or manned submersibles to deploy a long-baseline instrument; however, such equipment is costly to operate and requires access to a specialized ship. To facilitate our design and test program, we chose to use the dynamic deployment technique which *Webb et al.* [1985] developed for long electromagnetic sensors. At sea the sensor is released into the water from a reel, starting with the end pot assembly, with the ship traveling at about  $8 \text{ m s}^{-1}$ . The drag force associated with the ship

motion keeps the tiltmeter tubing nearly level (important if the pressure gauge and end pots are not to be overpressured) and prevents crimping the tubing during deployment. When the full length of the tiltmeter is nearly paid out, we make the electrical and physical connections between the tubing/sensor package and the data logger and heavy anchor assembly. The anchor is connected to an electromechanical cable such as a conductivity-temperature-depth cable, which is itself terminated by an acoustic transponder/release system, allowing us to monitor the height above the seafloor during deployment (i.e., a standard deep-towed instrument arrangement). We then lower the logger and tubing assembly to near the seafloor, using the cable, and when the entire package (the full length of the tiltmeter) is about 15 m from the seafloor, we release the instrument to settle under its own weight.

Acoustic transponders that operate at 12 kHz are attached to the end pot assembly and the logger assembly (i.e., the two ends of the tiltmeter) and allow us to measure the deployed length and the depths of the ends of the tiltmeter by an acoustic survey. The instrument then operates on the seafloor for the duration of the experiment. At the end of the recording period an acoustic command to the data logger initiates release from the logger anchor, and the insulated wires connecting the sensor block (which is secured to the anchor) to the logger are broken, allowing the logger package to rise to the surface under its own buoyancy.

## Costs

It is relevant to discuss the costs to deploy such an instrument. There are three main components to the

**Table 1.** Physical Properties of Tiltmeter Materials

Material	$\rho^a$	$\beta^b$	$\rho\beta$	C <sup>c</sup>	Source
Ethylene glycol (25 °C)	1.1099	5.713	0.6341	3.7	<i>Washburn</i> [1930]
Ethylene glycol (0 °C)	1.1257		0.6431	3.5*	<i>Washburn</i> [1930]
Ethylene glycol (0 °C, 15 MPa)	1.1313 <sup>†</sup>		0.6463	3.3*	<i>Washburn</i> [1930]
Isopropanol (0 °C)	0.8014	8.09	0.6483	8.4	<i>Washburn</i> [1930]
Isopropanol (0 °C, 15 MPa)	0.8110 <sup>†</sup>		0.6561	7.9*	<i>Washburn</i> [1930]
122 alloy copper tubing	8.94	0.177			<i>Boyer and Gall</i> [1985]
Aluminum end pots	2.73	0.226			<i>Boyer and Gall</i> [1985]

<sup>a</sup>Density ( $10^3 \text{ kg m}^{-3}$ )

<sup>b</sup>Thermal expansivity (volumetric for fluids, linear for solids) ( $10^{-4} \text{ K}^{-1}$ )

<sup>c</sup>Compressibility ( $10^{-4} \text{ MPa}^{-1}$ )

\*Estimate from data at 25–100 °C and 0.1, 50 and 100 MPa

<sup>†</sup>Estimate using compressibility

system: the sensor and anchor assembly, the data logger, and the acoustic navigation and release device.

Parts, machining and labor for the sensor components cost about \$5000, including the Validyne gauge, which amounts to about one sixth of this cost. Sensor cost depends somewhat on the materials used; copper tubing and aluminum parts can be employed for short deployments, while more costly stainless steel or titanium parts would be needed for observatory installations. Acoustic navigation/release systems can be purchased commercially for around \$10,000; we build our own devices in-house for about one third this cost. Low-power, seafloor data loggers capable of recording for a year or more are currently not commercially available. A more modern version of the logger used for the experiment described in this paper is currently being constructed in-house for about \$7500 in parts.

The total cost of parts, machining, and batteries amounts to less than \$15,000 per LBT, which compares favorably with short-baseline instruments, as the logger and release components are essentially the same and the sensor costs are comparable. The deep-towed deployment scheme requires more time (about 5 hours per instrument) and a somewhat more capable ship than does simply dropping instruments from the surface (which requires about 2 hours per instrument if they are tracked to the seafloor), but in either case the time required and costs involved in getting to, conducting bathymetric surveys of, and returning from the research area usually greatly exceed the time and costs involved in deploying the instruments.

The logger and release system are recovered and are reusable. For the deployments that were part of the development cycle (and the experiment we describe below) the anchor and sensor assembly are left on the seafloor. We have experimented in providing extra buoyancy and

lifting the sensor back to the surface, but the long tube assembly tends to foul and catch on rocks, endangering our ability to recover the data. However, we have also experimented with providing an underwater matable electrical connector on the tiltmeter sensor, allowing a working tiltmeter sensor to be reoccupied by using a submersible to connect a second data logger.

## Juan de Fuca Ridge Experiment

Axial Seamount is a volcano of the Cobb-Eickelberg Seamount Chain, located at the intersection with the Juan de Fuca Ridge (JDF) approximately 450 km west of the Washington-Oregon border (see Figure 3 inset) [Johnson, 1993]. The volcano has an elongated summit caldera measuring about 3 by 8 km, with its long axis oriented N160° [Embley et al., 1990]. Its highest elevation is on the western edge of the caldera, where the volcano rises approximately 700 m above the surrounding ridge axis.

We deployed six short- and four long-baseline tiltmeters on Axial Seamount (see Figure 3) from June 29 to September 8, 1994; these instruments collected approximately 65 days of continuous data on five short-baseline instruments and one long-baseline tiltmeter. Minor but correctable problems (an incorrect hard disk SCSI ID, a blown fuse, and a faulty release system) prevented us from collecting data from the other three long-baseline instruments. We also deployed three electric and magnetic field recorders for a magnetotelluric survey; these data have been analyzed elsewhere [Heinson et al., 1996]. In total we collected 30 channels of short-baseline tilt, one channel of long-baseline tilt and the associated temperature record, nine magnetic field records, six electric field records, five hydrophone recordings, and 15 channels of seismic data. Here we

present analysis of data pertinent to stability and performance of our long-baseline tiltmeter. More details on the short-baseline instruments are presented by *Wyatt et al.* [1996] and Tolstoy et al. (submitted manuscript, 1997).

## Results and Discussion

For the Juan de Fuca Ridge experiment we used the logging system described by *Constable and Cox* [1996], which utilizes Onset Corporation's CPU8088 microcomputer along with voltage-controlled oscillators and 16-bit counters to effect 16-bit analog-to-digital conversion with a least count of 0.1 Pa or  $0.33 \mu\text{rad}$ . Data were collected at a sampling rate of 1 Hz and, during later processing, were block averaged to hourly samples. Figure 4a shows the raw hourly block-averaged data from the long-baseline tiltmeter Rhonda; signals with several different characteristic timescales, ranging from DC to minutes, are evident. First, there is a DC level of about 40 mrad, which corresponds to a height difference of 4 m between the end pots and the pressure sensor; this value is in excellent agreement with an acoustic survey of the instrument made after its deployment. After about 10 days of rapid instrument settling a long-term variation can be seen with a tilt rate of  $5 \mu\text{rad day}^{-1}$  near the beginning of the record, decreasing to about  $0.5 \mu\text{rad day}^{-1}$  by about day 240. This decreasing drift signal is likely due to continued instrument settling, although instrument drift or volcanic tilt could also cause the final observed variation. There are two abrupt offsets in the record with amplitudes of 56 and  $19 \mu\text{rad}$  (5.6 and 1.9 mm relative height change over the 100-m instrument baseline), respectively. These offsets occur over a timescale of a few minutes and are thus distinct from volcanic deflation events, which typically have timescales of hours to days; we believe that these sharp drops are caused by settling of the end pots or sensor block, as might be expected on unconsolidated oceanic crust. However, they also might possibly be associated with mechanical or electronic instrument tares. Finally, there is an approximately tidal variation present throughout Rhonda's recording. To analyze this last signal more closely, we have removed the long-term drift, using a best-fit depleted-basis B-spline [*Constable and Parker*, 1988]. The resulting residual tilt is shown in Figure 4b and displays a mean amplitude of about  $\pm 6 \mu\text{rad}$ , much higher than the  $0.2 \mu\text{rad}$  expected tidal tilt (Tolstoy et al., submitted manuscript, 1997); we explore several explanations to explain these high-frequency signals, since it is clear that they are not primarily tidal tilt.

Rhonda's temperature record is shown in Figure 4c; oscillations of the order of  $\pm 0.05 \text{ K}$  are evident. We compute estimates of the coherence between tilt and temperature using both conventional Welch's overlapping segment averaging [*Percival and Walden*, 1993]

and multitaper techniques [*Park et al.*, 1987; *Vernon et al.*, 1991]; we note no significant differences between the estimates. Figure 5a shows the coherence estimate and the 95% and 99% significance levels computed non-deterministically by using a method adapted from that of *Kuehne et al.* [1993]. Highly significant coherence is evident in three broad frequency bands (0.2–0.5, 0.8–1.3, and 1.5–2.4 cycles/day (cpd)), which indicates that there is a component to the tilt data that is either driven by temperature or driven along with temperature by a third phenomenon.

We estimate the temperature-to-tilt transfer function to give an upper bound on the apparent temperature coefficient of our tiltmeter (see Figure 5b); our computed value is  $70 \pm 30 \mu\text{rad K}^{-1}$  from 8 hours to 10 days period. The phase of the transfer function estimate, shown in Figure 5c, is linear from 5 to 48 hours period; a linear phase relationship indicates a simple time offset between the two signals [*Priestley*, 1981], and from the slope of the transfer function phase we find that tilt leads temperature by about 40 min.

Our tiltmeter's "temperature coefficient" is much larger than we expect from (2), and we have considered several possibilities to explain this. First, if  $\rho\beta$  for the tiltmeter fluids under high pressure is sufficiently different from  $\rho\beta$  under atmospheric conditions, the temperature compensation in our design could be lost. However, since published values of  $\rho\beta$  for fluids similar to those used in our tiltmeter show pressure effects of less than 3%, and we compute from (2) that  $\rho\beta$  would have to change by over 400% to explain the observations, we reject this pressure effect as an explanation for the high "temperature coefficient." Another possibility is that one of the tiltmeter tubes tubes crimped closed during deployment. We reject this on the grounds that the design of our tiltmeter makes it unlikely that one tube could crimp closed, that the excellent agreement between the DC tilt offset and the acoustic survey of the instrument indicates that the tiltmeter was operating correctly, and that the coherence between temperature and tilt would be much higher and broadband (since a fluid tube tiltmeter with one arm closed is essentially a thermometer). The final and perhaps most compelling argument against temperature-driven "tilt" is that the phase of our transfer function estimate indicates that tilt leads temperature by 40 min, precisely the opposite of what one would expect if temperature drove tilt. While this lag could be explained by differences in the rates of heat diffusion in the tiltmeter fluids and the plastic insulation on the telephone cable, simple diffusion calculations using published values of thermal conductivity for the materials involved show that the maximum expected lag would be 50 s, with temperature leading tilt.

We conclude from the above that temperature is not driving tilt but that both temperature and differential

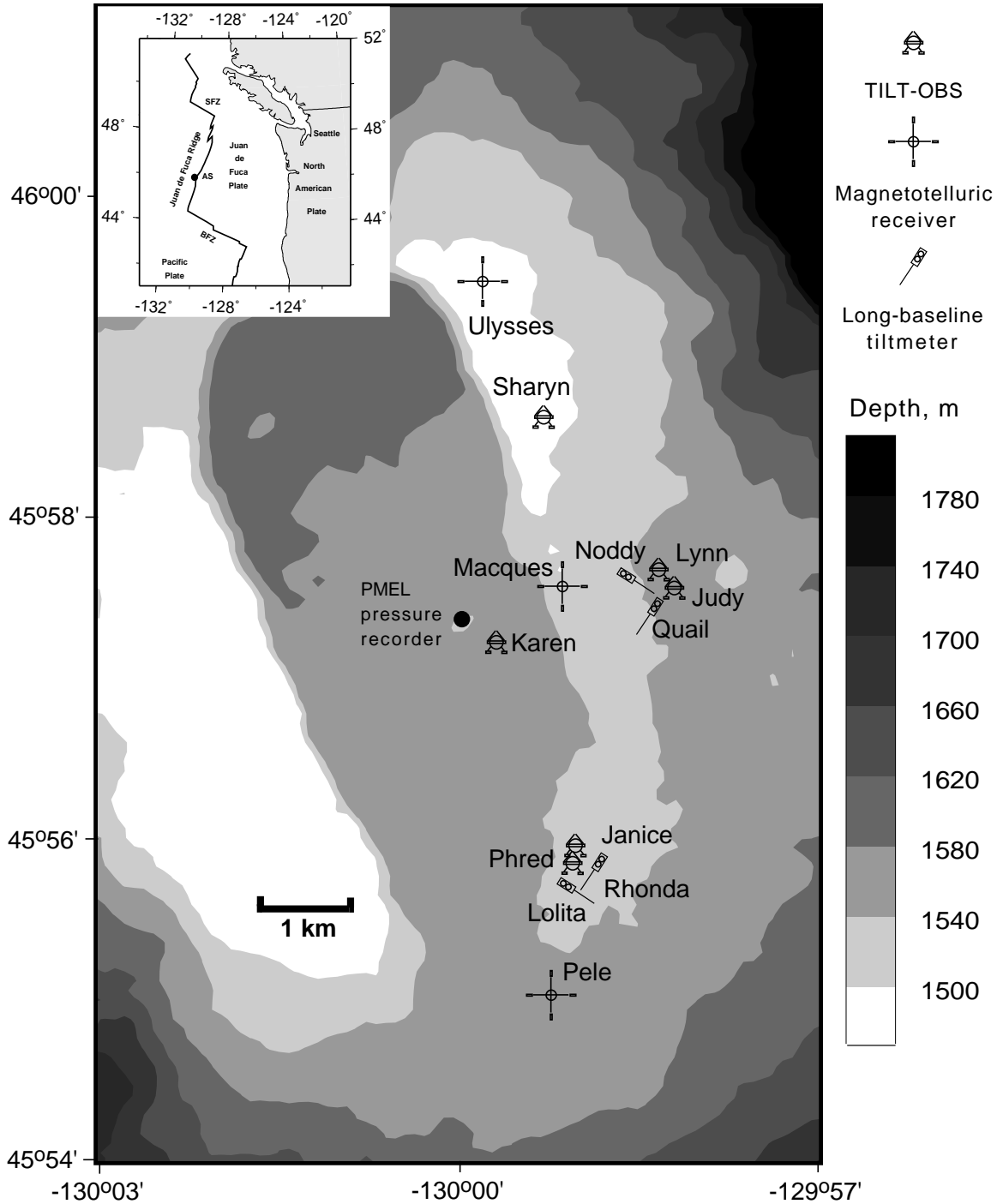


**Figure 3.** Map of the summit of Axial Seamount showing deployment locations for the 1994 experiment. Rhonda, Lolita, Noddy, and Quail are LBTs; Janice, Phred, Judy, Lynn, Karen, and Sharyn are TILT-OBS; and Pele, Macques, and Ulysses are electric field instruments. The solid circle denotes the location of the PMEL bottom pressure recorder. Scale is shown in the lower left corner, and bathymetry is indicated by the shading, with lighter shades denoting shallower depths. Inset map shows the location of Axial Seamount and the Juan de Fuca Ridge in relation to the northwest coast of North America. Axial Seamount is denoted by the black circle labeled AS; other abbreviations are Blanco Fracture Zone (BFZ) and Sovanco Fracture Zone (SFZ).

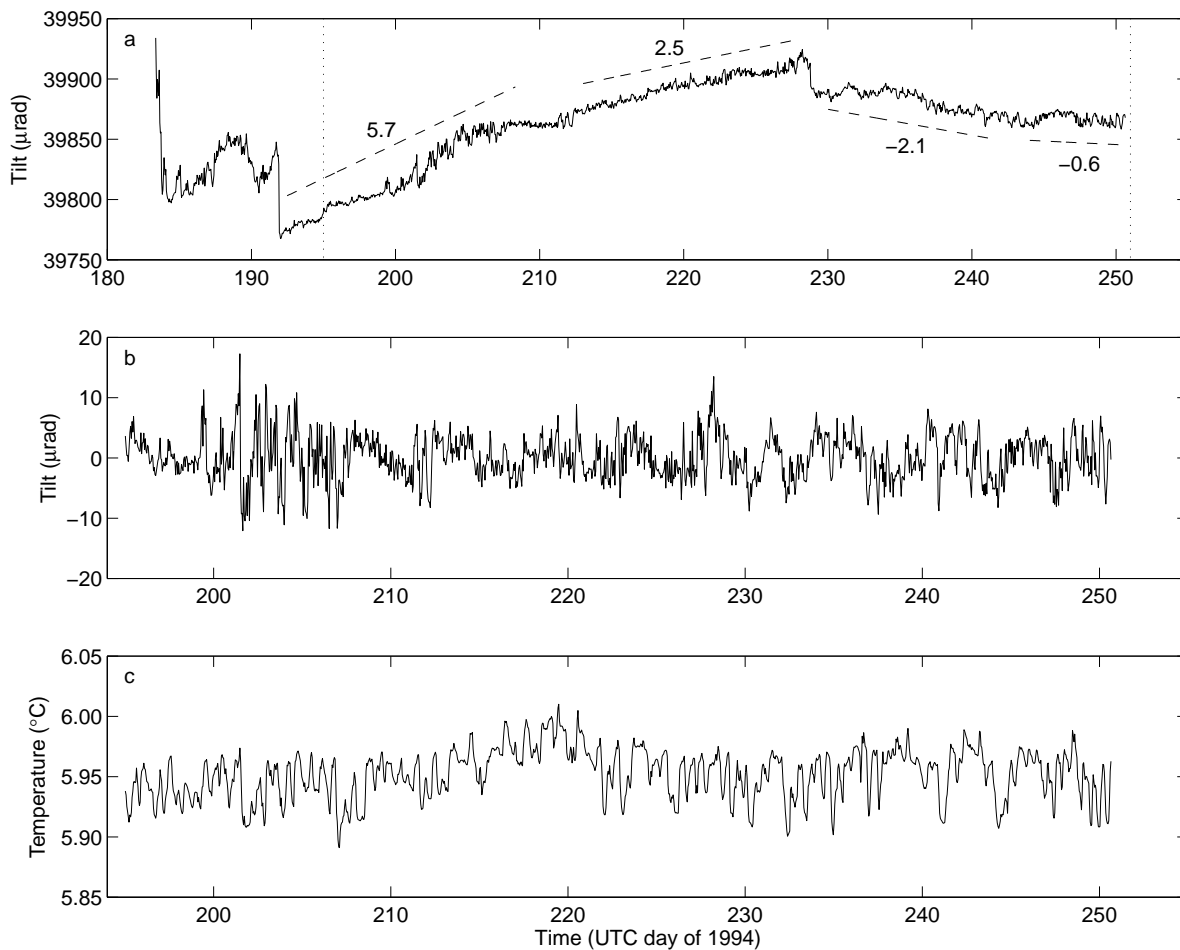


**Figure 4.** (a) Raw tilt data from Rhonda LBT. Signal prior to day 195 is largely rapid postdeployment instrument settling. Offsets at days 191 and 228 are likely due to settling or other instrument instability. Drift rates are indicated with dashed lines above and below tilt record: 5.7, 2.5, -2.1, and  $-0.6 \mu\text{rad day}^{-1}$ , respectively. Higher-frequency (approximately tidal) noise of about  $\pm 6 \mu\text{rad}$  is evident. Vertical dotted lines indicate the range of data shown in Figures 4b and 4c. (b) Residual tilt data from Rhonda LBT after correction of the offsets at days 191 and 228 and removal of a best-fit spline to eliminate the low-frequency variation. Data prior to day 195 (which are contaminated by deployment-related noise) have been dropped. Noise at about  $\pm 6 \mu\text{rad}$  is visible. (c) Raw temperature record from Rhonda LBT. Variations of the order of  $\pm 0.05 \text{ K}$  are evident.

pressure (and thus tilt in our instrument) are being driven by a third common phenomenon. Since our estimates of the power spectra for tilt and temperature show peaks at the periods of the diurnal and semidiurnal tides (frequencies of 1.003 and 1.932 cpd, respectively), we examine the possibility that tidal absolute ocean height changes are the driving force. Data from a bottom pressure recorder (BPR) on Axial Seamount [Fox, 1990, 1993] show a strong tidal signature with an amplitude of about  $\pm 15 \text{ kPa}$  (Figure 6a). Because the BPR data are effectively tidal (spectral amplitudes 7–8 orders of magnitude higher in tidal bands than outside those bands), and our LBT temperature and tilt data are much broader band than the BPR data, we conclude that bottom pressure is not the driving force for our data. However, from these BPR data and our LBT

record, we can estimate that the common mode pressure acceptance of our tiltmeter is no higher than one part in 50,000.

While the bottom pressure does not explain the apparent temperature coefficient, the BPR and LBT temperature data show some interesting similarities. Figure 6b shows the temperature record from the BPR, and Figure 6c shows the BPR temperature record overlain with our LBT temperature record (both signals have had their computed means removed). The temperature waveforms match very well, except for an apparent time offset of 8–12 hours with Rhonda’s temperature leading. This waveform agreement is an important confirmation that our temperature measurement method works.

Ocean currents could drive the observed temperature

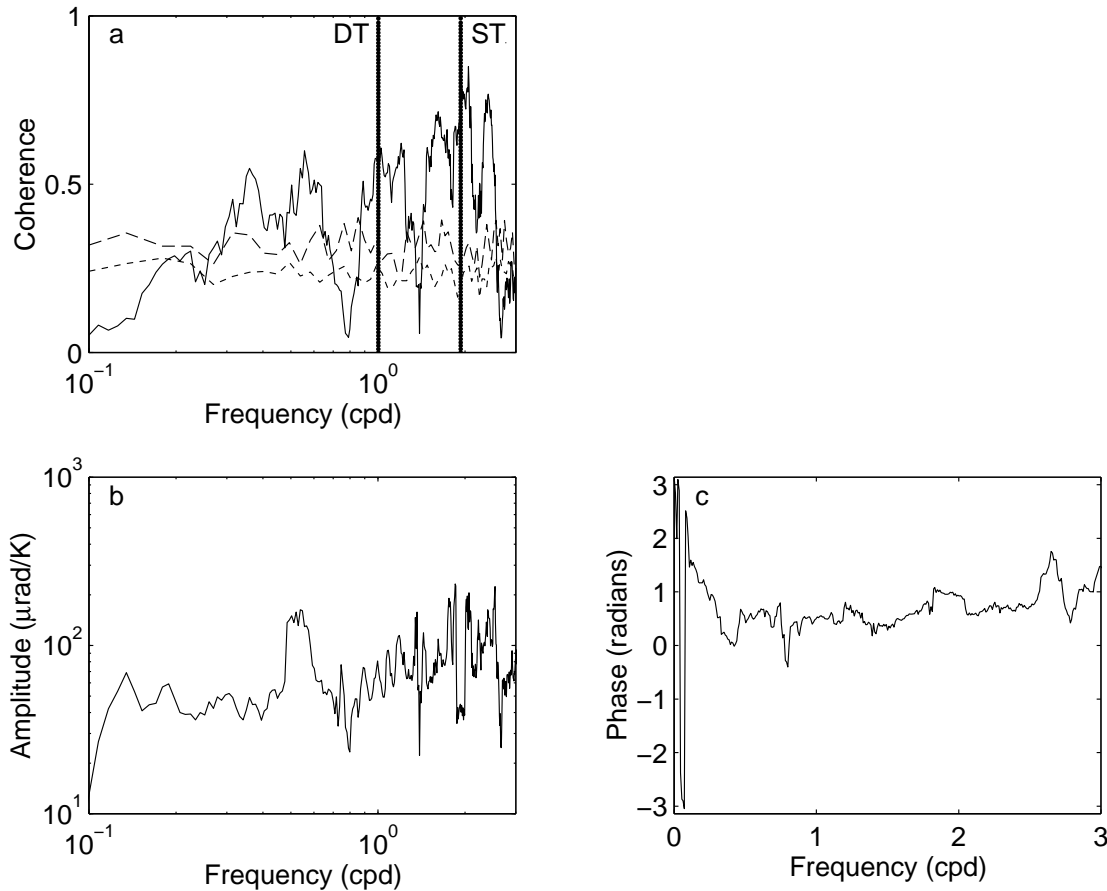


**Figure 5.** (a) Estimate of coherence between Rhonda LBT tilt and temperature (solid line). Short-dashed line is the 95% significance level, and long-dashed line is the 99% significance level. Note coherence significant at the 99% level in three broad bands, surrounding the diurnal and semidiurnal tides (lines labeled DT and ST, respectively) and the 4-day oscillation. (b) Amplitude spectrum of the transfer function from temperature to tilt. (c) Phase spectrum of the transfer function. Note the linearity from about 0.5 to 3 cpd.

and tilt signals. Currents could drive temperature fluctuations either by modulating the rate of heat loss from the volcano or by moving parcels of relatively warm or cool water over the tiltmeter; either mechanism could explain the time offset between the LBT and BPR temperature records. A spurious apparent tilt signal could result from current-driven wobbling of the bulky end pot assembly or wiggling of some part of the tiltmeter tubing.

Seafloor electric field variations in the frequency band of interest (up to the semidiurnal tide) are primarily driven by barotropic ocean motions coupling through the Lorentz force ( $\mathbf{E} = \mathbf{v} \times \mathbf{B}$ ) [Filloux, 1987] so we may use the electric field records we collected during our experiment as a proxy for ocean currents to test the current-forcing hypothesis. Figure 7a shows the electric fields recorded by Ulysses, Macques, and Pele after a best-fit spline is removed and after rotation to

a common orientation (rotation angles determined by Heinson *et al.* [1996]; channel 1 is north positive). The residual electric field shows a tidal signature with typical variations of the order of  $\pm 3 \mu\text{V m}^{-1}$ , which can be converted to current speeds of about  $5\text{--}10 \text{ cm s}^{-1}$ . Multitaper estimates of coherence and cross spectra show high coherence between instruments with zero relative phase, which indicates that all three instruments were recording the same signal.

Figure 7b shows representative electric field spectra (from Macques), while Figure 7c shows a spectrum of current velocity data from Cannon and Pashinski [1990] for comparison. Both spectra exhibit similar peaks at frequencies of about 1, 1.5, and 2 cpd with a broad peak centered near 0.25 cpd. The peaks at 1 and 2 cpd correspond to tidal currents at the periods of the diurnal and semidiurnal tides, respectively, while the peak at 1.5 cpd corresponds to Coriolis-coupled wind-

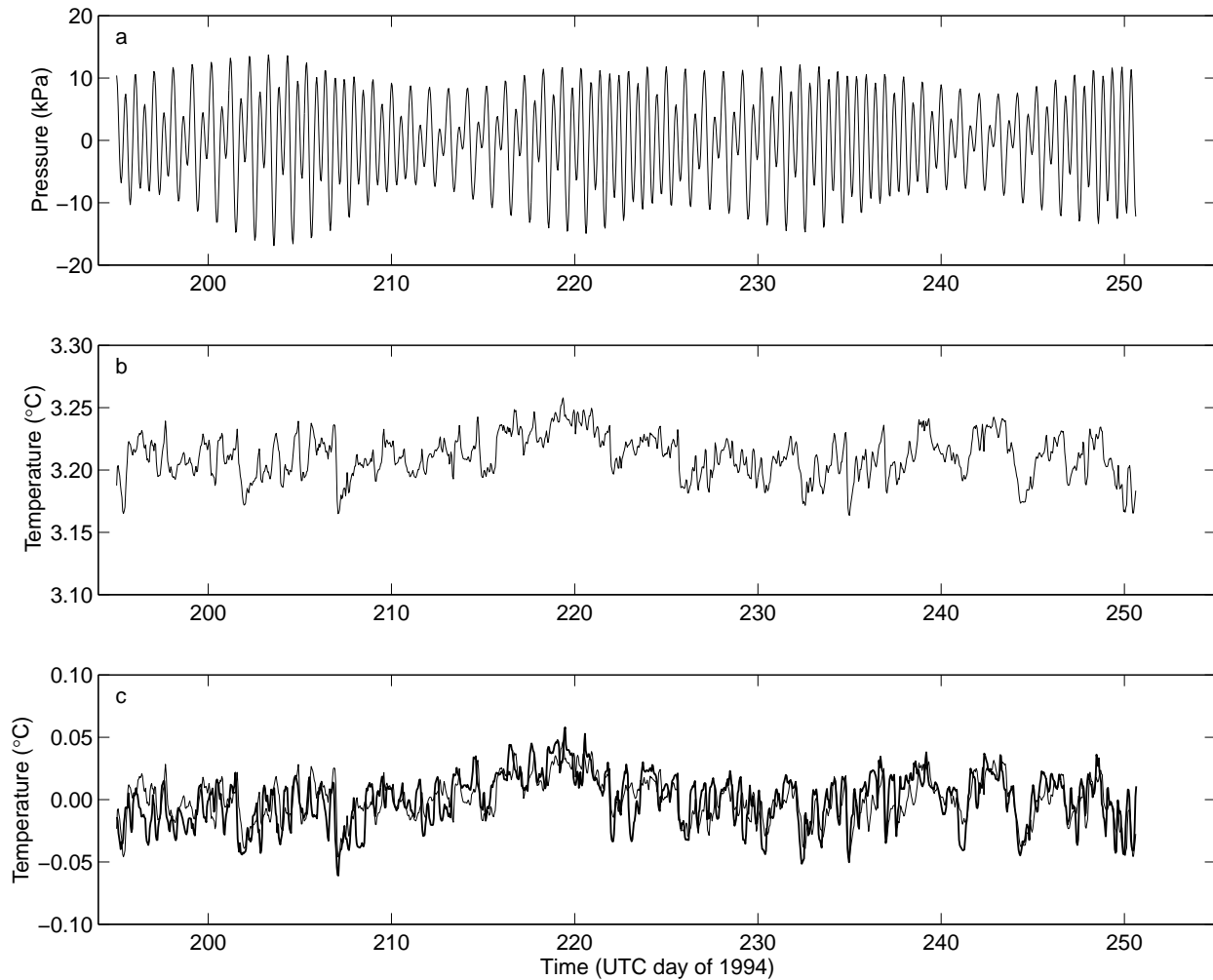


**Figure 6.** (a) Bottom pressure recording from the PMEL BPR. (b) Bottom temperature record from the PMEL BPR. Note oscillations of the same order as those on the LBT temperature record, but with a different mean value. (c) LBT temperature record (thick line) and BPR temperature data (thin line). Note the excellent agreement between the records except for a time offset of approximately 8–12 hours with the LBT temperature leading. Both signals have had their computed means removed.

driven currents. *Cannon and Thomson* [1996] identify the broad peak at about 0.25 cpd as delineating currents driven by local weather; these currents interact with the rough topography of the JDF to create northward propagating ridge-trapped waves, which travel at about  $1 \text{ m s}^{-1}$ . The peak at 3 cpd is due not to currents but to the geomagnetic solar daily variation [Filloux, 1987]. This comparison confirms that our electric field measurements reflect the ocean currents in our deployment area at periods longer than 8 hours.

We test for ocean current forcing by estimating coherences between the temperature and tilt data from Rhonda and the electric field records from the nearest electromagnetic instrument, Pele. We observe moderately strong coherence between the electric field and LBT temperature record in the semidiurnal tidal frequency band as well as significant, but lower, coher-

ence in the diurnal tidal, inertial, and 4-day oscillation bands. We also note significant, though weaker, coherence between tilt and the electric field, particularly in the semidiurnal tidal band; this weak coherence might be partially governed by the 2-km physical separation between Pele and Rhonda. We conclude that ocean currents are at least partially responsible for apparent tilt as recorded by our long-baseline tiltmeter but that other as yet undetermined forces are also driving the observed tilt.

### Comparison With Short-Baseline Seafloor Tiltmeters

If currents are at least partially responsible for apparent tilt in our long-baseline tiltmeter, currents should have an appreciable effect on the short-baseline tiltmeters we deployed. Figure 8a shows the residual tilt

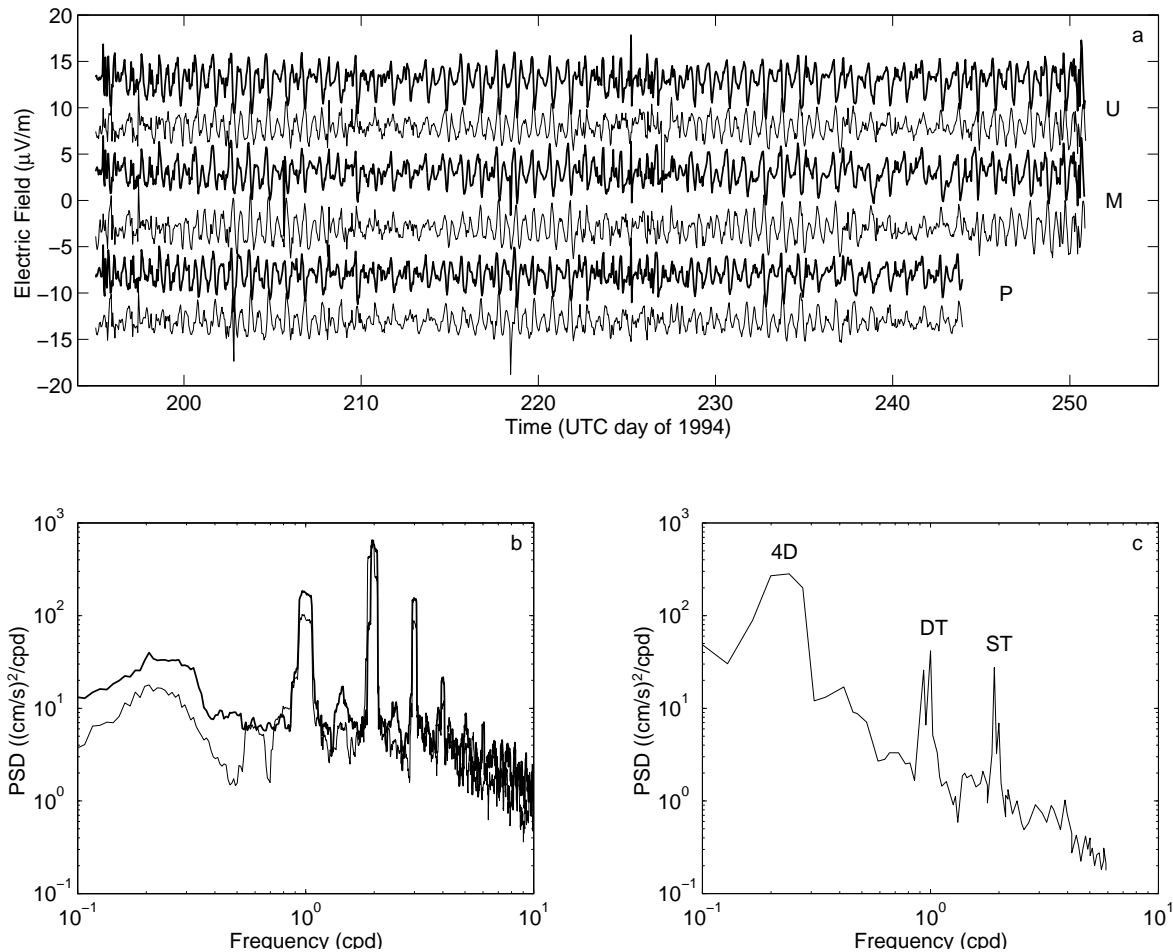


**Figure 7.** (a) Residual electric field data from Ulysses, Macques, and Pele after removal of a best-fit spline and rotation to a common orientation. Thick line is north component, and thin line is east component. Variations of the order of  $\pm 3 \mu\text{V/m}$  are evident. Note similarity of records across instruments. (b) Power spectrum of Macques electric field converted to ocean current speed. Thick line is north, and thin line is east. Note strong peaks at 1, 1.5, 2, and 3 cpd and broad peak centered at 0.25 cpd. The peaks at 0.25, 1, 1.5, and 2 cpd are due to ocean currents. (c) Power spectrum of measured current speeds near Axial Seamount. Peaks at 0.25 cpd and the frequencies of the diurnal and semidiurnal tides are denoted 4D, DT, and ST respectively. Note the similarity to Macques electric field in Figure 7b. After *Cannon and Pashinski* [1990].

from these four instruments after a best-fit spline has been removed (Tolstoy et al., submitted manuscript, 1997), with the long-baseline tilt data from Rhonda shown for comparison. On three of the short-baseline tiltmeter records, tidal oscillations of the order of  $\pm 5 \mu\text{rad}$  are evident. The fourth instrument, Karen, was deployed inside the summit caldera and shows a noise signature much reduced in relation to that of the other instruments. The lower noise levels on Karen are consistent with the interpretation that currents are rocking the tiltmeters, as Karen would be relatively sheltered inside the caldera and thus would be moved less than the other tiltmeters.

Figure 8b shows representative power spectra for the short-baseline tilt data from Judy. Both spectra (X and Y component) exhibit distinct diurnal and semid-

urnal tidal peaks, as one might expect if these instruments were recording earth tides. However, the inertial peak at 16.7 hours period and the 4-day oscillation are also evident in the spectra from the short-baseline tiltmeters that were installed on the caldera rim. These two peaks are current-related [*Cannon and Pashinski*, 1990], and given that these instruments are not perfectly coupled to the seafloor, it is reasonable to conclude that some current-driven wobbling is contained in the short-baseline tilt records.

If currents are rocking both the short- and long-baseline tiltmeters, the time series recorded by these instruments should be coherent at frequencies outside the known tidal bands. Unfortunately, the short-baseline tiltmeter nearest Rhonda is Janice, which did not give useful recordings, and the next nearest, Phred, recorded

too few data to give reliable coherence estimates. We are reduced to using data from the next nearest instrument, Judy, which is 3.5 km away. The coherence between Judy's tilt and Rhonda's tilt depends on component and is not very strong, but it is significant at the 99% level in the 4-day band and the inertial band, as well as the diurnal and semidiurnal tidal bands. There are qualitative similarities as well; Figure 8a shows that the increased noise on Rhonda's record from about days 198–207 is also evident on Judy and Lynn. It is thus reasonable to suggest that currents are rocking both the short-baseline tiltmeters and Rhonda, contributing high-frequency noise to the data recorded by both kinds of instruments.

It is apparent from Figure 8a that our long-baseline tilt data have a high-frequency noise level that is only about a factor of 2 larger than that of the short-baseline data; how do the long-term drift rates compare? Tolstoy et al. (submitted manuscript, 1997) estimate the drift rates (after the initial instrument settling) for the short-baseline tiltmeters to range from about 1 to 10  $\mu\text{rad day}^{-1}$ ; these values are comparable to the drift rates in our long-baseline data (0.5–5  $\mu\text{rad day}^{-1}$ ). In both cases the drift rates decline with time. However, the character of the decline is fundamentally different: the SBT data stabilize quasi-exponentially, while the LBT data tend to exhibit stable tilt rates, punctuated by abrupt offsets, after which tilt continues at a different (lower) rate. Eventually, both the short- and long-baseline tiltmeters are likely to reach some low stable tilt rate.

## Comparison With Subaerial Volcanic Tilt Observations

The long-baseline tilt data from Rhonda exhibit long-term drift rates of 5  $\mu\text{rad day}^{-1}$  near the beginning of the record, decreasing to less than 1  $\mu\text{rad day}^{-1}$  near day 240, as well as a higher-frequency noise level of about  $\pm 6 \mu\text{rad}$ . Given these drift rates and noise levels, it is important to ask whether or not we would be able to detect known volcanic signals with this instrument; we may appeal to long time series of tilt recorded on active subaerial volcanoes to address this question.

The best such long-term record is that from the open-ended fluid tube tiltmeter operated at Uwekahuna vault (about 300 m from Kilauea Caldera) by the Hawaii Volcano Observatory. Figure 9a shows a 32-year record from the Uwekahuna LBT. Steady rises over several months, reflecting slow inflation of a shallow magma chamber, are plainly evident. These rises are punctuated by abrupt drops in tilt, which correspond to catastrophic deflation of the volcano during eruption or drainage of the central magma chamber into a flank or rift zone reservoir.

We have computed daily first differences of the Uwe-

kahuna tilt record to give an estimate of the background noise observed while operating a long-baseline tiltmeter on an active volcano, as well as to quantify the tilt rates associated with eruptive or intrusive deflation events (Figure 9b); histograms of these first differences are shown in Figures 9c and 9d. The mean daily variation observed in the Uwekahuna record is 0.02  $\mu\text{rad day}^{-1}$ , with a scatter of about 3.2  $\mu\text{rad day}^{-1}$ , which reflects background ground and instrument noise. Closer examination of the tilt rates (Figures 9b and 9d) shows many high tilt rate events, primarily deflations, corresponding to eruptive or intrusive episodes at Kilauea. The largest of these events have tilt rates that can exceed 100  $\mu\text{rad day}^{-1}$ , with many more moderate events displaying tilt rates of greater than 10  $\mu\text{rad day}^{-1}$  [e.g., Duffield et al., 1976; Moore et al., 1980; Decker, 1987]. Smaller events almost certainly grade smoothly into the background noise on the record.

In Figures 9b and 9d we have indicated the  $\pm 6 \mu\text{rad}$  high-frequency noise seen on our LBT record as a visual measure of the ability of our instrument to record these eruption signatures. While the background daily tilt on Kilauea is roughly half that of our current instrument, it is clear that moderate to large volcanic events at Kilauea have tilt rates well above the drift rates and noise levels we observe in our record of long-baseline tilt. The fact that we did not record any eruptive signature at Axial Seamount suggests that no active eruption was occurring at the time of our deployment; data from the short-baseline tiltmeters, nearby independent bottom pressure recorders, and the U.S. Navy's Oregon SOSUS (SOUND SURVEILLANCE SYSTEM) arrays are in agreement with this interpretation. By combining our long- and short-baseline tilt records we can also bound the rate of inflation or deflation on Axial Seamount to be less than 0.5–1  $\mu\text{rad day}^{-1}$  during mid-1994.

## Future Directions

Although the necessity of developing and testing the new tiltmeter by actual deployment has made its development a long and difficult process, we have achieved notable success in that we have an instrument that not only works but is capable in principle of measuring the signal of interest. The cost and performance of the new tiltmeter are comparable to short-baseline tiltmeters, and because of its ability to measure a broad deformation field rather than local instabilities, a long-baseline tiltmeter is clearly a desirable instrument.

Given our understanding of the in situ instrument performance gained by the analysis presented in this paper, we would expect to achieve better noise and drift levels in future deployments of the tiltmeter, particularly those that are longer than the 2-month equilibration time of the instrument. As ocean currents appear to be a noise source in our tiltmeter, we could do two things to improve the seafloor coupling and reduce the

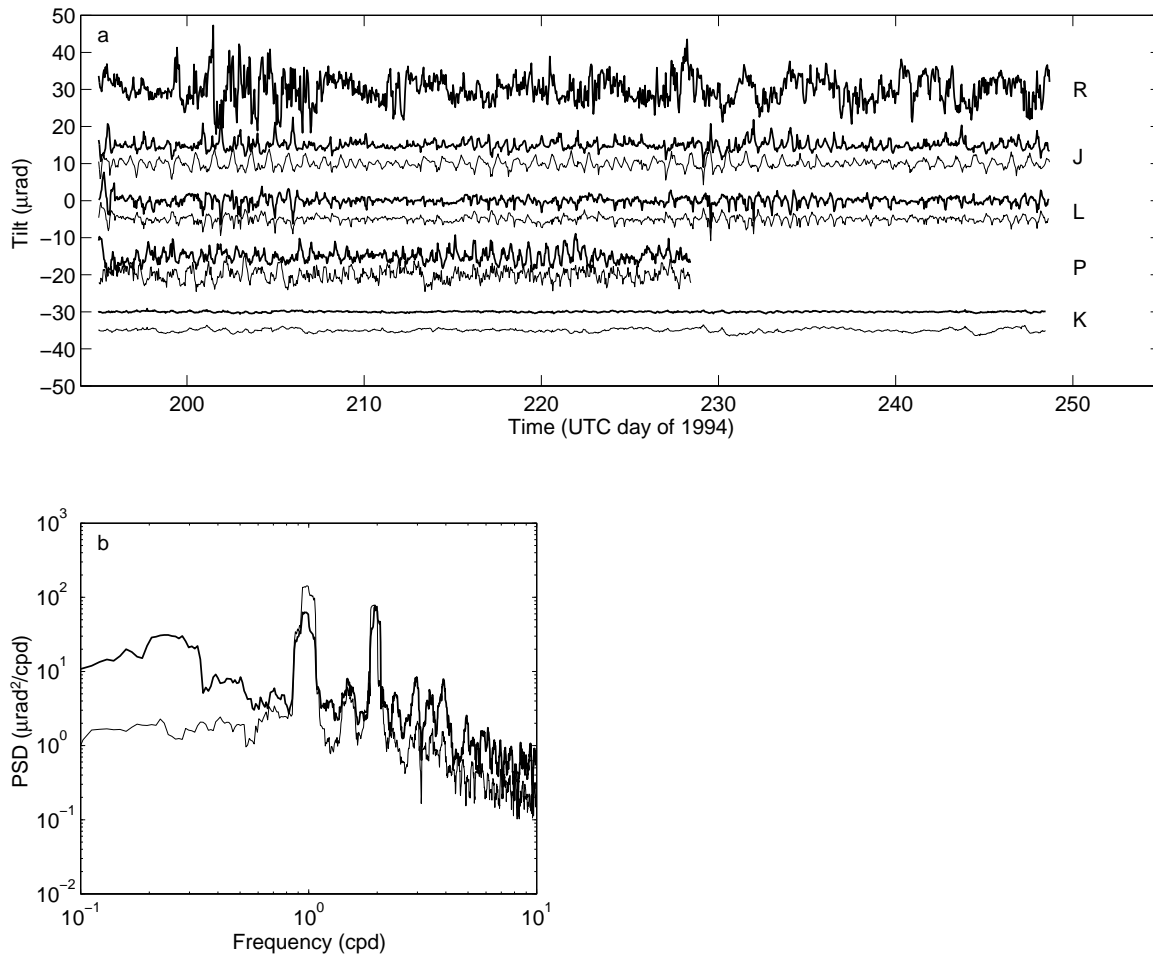


**Figure 8.** (a) Residual short-baseline tilt data from Phred, Judy, Lynn and Karen after removal of a best-fit spline. Thick line is X component, and thin line is Y component. Note that Karen's noise level is about 10 times lower than the levels of the other instruments, a decrease that may reflect that instrument's relatively sheltered location in the caldera. Rhonda LBT data are shown for comparison. (b) Power spectra for the short-baseline tiltmeter Judy. Thick line is X, and thin line is Y. Both spectra display the 4-day and 1.5 cpd oscillations, which are current driven.

current-driven noise: (1) the current generation of data loggers are about one third the size of the ones used on Axial Seamount and so will present a smaller cross section to ocean currents, and (2) the construction of the end pot assembly can be rationalized to make the assembly smaller, heavier, and radially symmetric. Data from ancillary sensors such as current meters or electrodes on the tiltmeter to measure water motion, thermistors at the pot and sensor ends to give point estimates of temperature to complement the integrated measure, and bottom pressure sensors of the type used on the BPR would help us to compensate for the effects of these sources of environmental noise.

There are fluids with densities greater than ethylene glycol (although they are generally harder to work with) that would provide larger pressure signals for a given tilt. While it is not yet clear what the optimal length of the tiltmeter is, longer instruments are likely to pro-

vide a better signal-to-noise performance. The maximum practical instrument length is limited by seafloor roughness but in any case probably will not exceed the water depth (usually in the range of 1 to 4 km).

It is currently technically infeasible to construct a seafloor tiltmeter (short- or long-baseline) that will be capable of recording tilt events with rates typical of continental-style plate boundary tectonics; such signals are just too small in relation to instrument and environmental noise. However, tilt rates associated with eruptive or intrusive events at subaerial volcanoes are several orders of magnitude larger than the rates observed at active continental plate boundaries and are within the reach of current technology. Potentially greater instability of volcanoes on relatively thin oceanic crust and similarities in magma emplacement rates between Hawaiian and MOR volcanoes may lead one to expect that MOR volcanoes would display deformation behav-

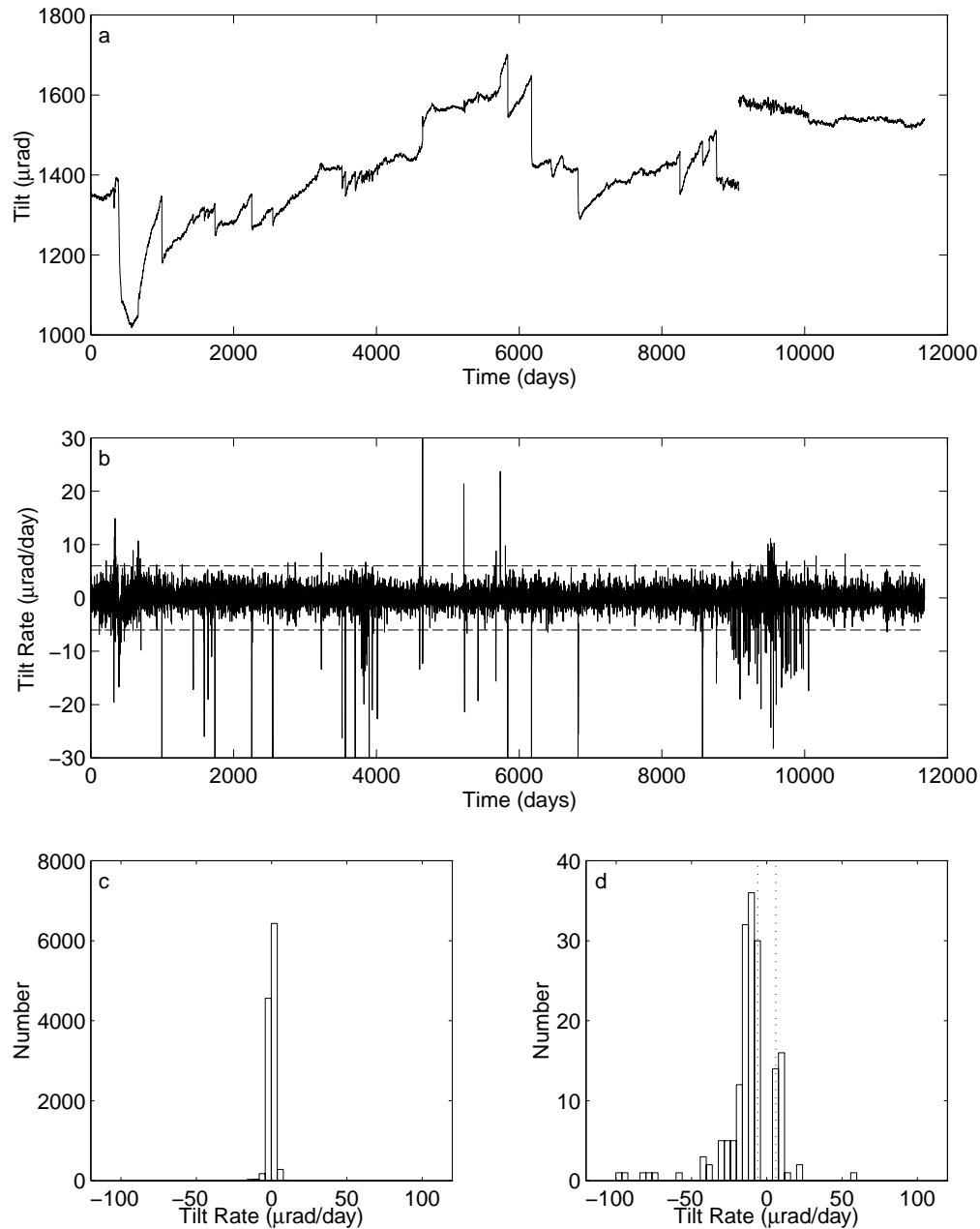


**Figure 9.** (a) Record of tilt from Uwekahuna vault at HVO. The break in the data at about day 9100 is due to operator intervention. Note steady long-term inflation punctuated by rapid tilt rates near eruptions. (b) Daily first differences of the data in Figure 9a. Dashed line is shown at  $\pm 6 \mu\text{rad}$  to reflect the typical high-frequency noise level observed on Rhonda. (c) Histogram of Figure 9b. (d) As in Figure 9c, except that only bins for tilt rates in excess of twice the standard deviation are shown. Note the high tilt rate events corresponding to eruptive inflation/deflation events. There are more than 30 events with deflation tilt rates in excess of  $20 \mu\text{rad day}^{-1}$ . Dotted lines are shown at  $\pm 6 \mu\text{rad}$  for comparison.

ior similar to that of subaerial volcanoes, but this theory still has to be verified through direct observation. These arguments and the data presented in this paper lead us to conclude that the long-baseline instrument described in this paper is capable of recording rapid volcanic tilt on seamounts or active MOR segments. Long-duration monitoring experiments using both improved tiltmeters and ocean bottom seismographs are necessary to provide order-of-magnitude bounds on the deformation at and the eruptive behavior and internal structure and dynamics of active submarine volcanoes.

**Acknowledgments.** Tom Deaton and Jacques Lemire provided technical support. We thank the captain and crew of R/V *Wecoma* for support in both the deployment and recovery cruises and Chris Fox and Harold Mofjeld for providing pressure and temperature data. Deployment of the short-baseline tiltmeters was conducted in collaboration with Maya Tolstoy and John Orcutt, who also gave helpful advice and criticism. We thank Roger Denlinger for supplying the Uwekahuna LBT tilt record. Paul Davis kindly provided computer codes for computing the prolate spheroid-driven deformation field. We thank Roger Bilham, David Clague, Megan Flanagan, and Alan Linde for insightful criticisms which improved this paper. This work was supported by NSF grants OCE-8911428 and OCE-9200879.

## References

- Agnew, D. C., Strainmeters and tiltmeters, *Rev. Geophys.*, *24*, 579–624, 1986.
- Baragar, W. R. A., M. B. Lambert, N. Baglow, and I. Gibson, Sheeted dykes of the troodos ophiolite, cyprus, in *Ernst et al.* [1987], pp. 257–272.
- Beavan, J., and R. Bilham, Thermally induced errors in fluid tube tiltmeters, *J. Geophys. Res.*, *82*, 5699–5704, 1977.
- Boyer, H. E., and T. L. Gall (Eds.), *Metals Handbook*, pp. 49–52 7–2, American Society for Metals, Metals Park, Ohio, 1985.
- Bradner, H., J. G. Dodds, and R. E. Foulks, Investigation of microseism sources with ocean bottom seismometers, *Geophysics*, *30*, 511–526, 1965.
- Cannon, G. A., and D. J. Pashinski, Circulation near axial seamount, *J. Geophys. Res.*, *95*, 12,823–12,828, 1990.
- Cannon, G. A., and R. E. Thomson, Characteristics of 4-day oscillations trapped by the juan de fuca ridge, *Geophys. Res. Lett.*, *23*, 1613–1616, 1996.
- Chadwell, C. D., F. N. Spiess, J. A. Hildebrand, L. Prawirodirdjo, L. E. Young, G. H. Purcell Jr, and H. Dragert, Juan de fuca geodesy project: Strain and plate motion measurement using gps and acoustics, *EOS Trans. AGU*, *76*, 1995, fall Meet. suppl., F412.
- Constable, C. G., and R. L. Parker, Smoothing, splines and smoothing splines: Their application in geomagnetism, *J. Comput. Phys.*, *78*, 493–508, 1988.
- Constable, S., and C. S. Cox, Marine controlled-source electromagnetic sounding, 2, the pegasus experiment, *J. Geophys. Res.*, *101*, 5519–5530, 1996.
- Davis, P. M., P. A. Rydelek, D. C. Agnew, and A. T. Okamura, Observation of tidal tilt on kilauea volcano, hawaii, *Geophys. J. R. Astron. Soc.*, *90*, 233–244, 1987.
- Decker, R. W., Dynamics of hawaiian volcanoes: An overview, in *Volcanism in Hawaii*, edited by R. W. Decker, T. L. Wright, and P. H. Stauffer, vol. 1350, pp. 997–1018, U.S. Geological Survey, 1987.
- Duffield, W. A., D. B. Jackson, and D. A. Swanson, The shallow, forceful intrusion of magma and related ground deformation at kilauea volcano, may 15–16, 1970, in *Proceedings of the Symposium on Andean and Antarctic Volcanology Problems*, edited by O. G. Ferran, pp. 577–597, Int. Assoc. of Volcanol. and Chem. of the Earth's Interior, Rome, 1976.
- Dvorak, J. J., A. T. Okamura, T. T. English, R. Y. Koyanagi, J. S. Nakata, M. K. Sako, W. R. Tanigawa, and K. M. Yamashita, Mechanical response of the south flank of kilauea volcano, hawaii, to intrusive events along the rift systems, *Tectonophysics*, *124*, 193–209, 1986.
- Dziak, R. P., C. G. Fox, and A. E. Schreiner, The june-july 1993 seismo-acoustic event at coaxial segment, juan de fuca ridge: Evidence for a lateral dike injection, *Geophys. Res. Lett.*, *22*, 135–138, 1995.
- Embley, R. W., K. M. Murphy, and C. G. Fox, High-resolution studies of the summit of axial volcano, *J. Geophys. Res.*, *95*, 12,785–12,812, 1990.
- Ernst, R. E., K. Bell, R. Ranalli, and H. C. Halls, The great abitibi dyke, southeastern superior province, canada, in *Mafic dyke swarms*, edited by H. C. Halls and W. F. Fahrig, vol. 34, pp. 123–135, Geological Survey of Canada, 1987, special Paper - Geological Association of Canada ; Vol. 34.
- Filloux, J. H., Instrumentation and experimental methods for oceanic studies, in *Geomagnetism*, edited by J. A. Jacobs, vol. 1, chap. 3, pp. 143–248, Academic Press, San Diego, Calif., 1987.
- Fox, C. G., Evidence of active ground deformation on the mid-ocean ridge: Axial seamount, juan de fuca ridge, april-june 1988, *J. Geophys. Res.*, *95*, 12,813–12,822, 1990.
- Fox, C. G., Five years of ground deformation monitoring on axial seamount using a bottom pressure recorder, *Geophys. Res. Lett.*, *20*, 1859–1862, 1993.
- Heinson, G., S. Constable, and A. White, Seafloor magnetotelluric sounding above axial seamount, *Geophys. Res. Lett.*, *23*, 2275–2278, 1996.
- Johnson, H. P., Processes associated with ocean crustal formation: The juan de fuca ridge, *Geophys. Res. Lett.*, *20*, 1847–1850, 1993.
- Johnson, R. V., C. R. B. Lister, and B. T. R. Lewis, A direct recording ocean bottom seismometer, *Mar. Geophys. Res.*, *3*, 87–102, 1977.
- Klein, F. W., Eruption forecasting at kilauea volcano, hawaii, *J. Geophys. Res.*, *89*, 3059–3073, 1984.
- Klein, F. W., R. Y. Koyanagi, J. S. Nakata, and W. R. Tanigawa, The seismicity of kilauea's magma system, in *Decker* [1987], pp. 1019–1185.
- Kuehne, J., S. Johnson, and C. R. Wilson, Atmospheric excitation of nonseasonal polar motion, *J. Geophys. Res.*, *98*, 19,973–19,978, 1993.
- Mogi, K., Relations between the eruptions of various volcanoes and the deformations of the ground surfaces around them, *Bull. Earthquake Res. Inst. Univ. Tokyo*, *36*, 99–134, 1958.

- Moore, R. B., R. T. Helz, D. Dzurisin, G. P. Eaton, R. Y. Koyanagi, P. W. Lipman, J. P. Lockwood, and G. P. Puniwai, The 1977 eruption of kilauea volcano, hawaii, *J. Volcanol. Geotherm. Res.*, **7**, 189–210, 1980.
- Park, J., C. R. Lindberg, and F. L. Vernon III, Multitaper spectral analysis of high-frequency seismograms, *J. Geophys. Res.*, **92**, 12,675–12,684, 1987.
- Percival, D. B., and A. T. Walden, *Spectral Analysis for Physical Applications: Multitaper and Conventional Univariate Techniques*, pp. 289–295, Cambridge Univ. Press, New York, 1993.
- Pollard, D. D., P. T. Delaney, W. A. Duffield, E. T. Endo, and A. T. Okamura, Surface deformation in volcanic rift zones, *Tectonophysics*, **94**, 541–584, 1983.
- Priestley, M. B., *Spectral Analysis and Time Series*, pp. 664, 681–685, Academic Press, San Diego, Calif., 1981.
- Rothery, D. A., The base of a sheeted dyke complex, oman ophiolite: Implications for magma chambers at oceanic spreading axes, *J. Geol. Soc. London*, **140**, 287–296, 1983.
- Sigurdsson, H., Dyke injection in iceland: A review, in *Ernst et al.* [1987], pp. 55–64.
- Sinha, M. C., D. A. Navin, L. M. MacGregor, S. Constable, C. Peirce, A. White, G. Heinson, and M. A. Inglis, Evidence for accumulated melt beneath the slow-spreading mid-atlantic ridge, *Philos. Trans. R. Soc. London, Ser. A*, **355**, 233–253, 1997.
- Staudigel, H., D. Agnew, S. C. Constable, C. Cox, J. Orcutt, G. Sasagawa, S. Webb, and F. Wyatt, In situ monitoring of microseismicity and tilt at mid ocean ridges: A progress report, *EOS Trans. AGU*, **71**, 1990, fall Meet. suppl., 1601.
- Vernon, F. L. I., J. B. Fletcher, L. Carroll, A. D. Chave, and E. Sembera, Coherence of seismic body waves from local events as measured by a small-aperture array, *J. Geophys. Res.*, **96**, 11,981–11,996, 1991.
- Washburn, E. W. (Ed.), *International Critical Tables of Numerical Data, Physics, Chemistry, and Technology*, vol. 3, pp. 27–42, McGraw-Hill, New York, 1930.
- Webb, S. C., S. C. Constable, C. S. Cox, and T. K. Deaton, A seafloor electric field instrument, *J. Geomagn. Geoelectr.*, **37**, 1115–1130, 1985.
- Westphal, J. A., M. A. Carr, W. F. Miller, and D. Dzurisin, Expendable bubble tiltmeter for geophysical monitoring, *Rev. Sci. Instrum.*, **54**, 415–418, 1983.
- Willoughby, D. F., J. A. Orcutt, and D. Horwitt, A microprocessor-based ocean-bottom seismometer, *Bull. Seismol. Soc. Am.*, **83**, 190–217, 1993.
- Wyatt, F., and J. Berger, Investigations of tilt measurements using shallow borehole tiltmeters, *J. Geophys. Res.*, **85**, 4351–4362, 1980.
- Wyatt, F., R. Bilham, J. Beavan, A. G. Silvester, T. Owen, A. Harvey, C. Macdonald, D. D. Jackson, and D. C. Agnew, Comparing tiltmeters for crustal deformation measurement: A preliminary report, *Geophys. Res. Lett.*, **11**, 963–966, 1984.
- Wyatt, F. K., S.-T. Morrissey, and D. C. Agnew, Shallow borehole tilt: A reprise, *J. Geophys. Res.*, **93**, 9197–9201, 1988.
- Wyatt, F. K., J. A. Orcutt, G. Sasagawa, H. Staudigel, and P. Zimmer, Toward in situ monitoring of active submarine volcanoes: A progress report, in *Fifth Circum-Pacific Energy and Mineral Resources Conference Transactions*, edited by G. P. Salisbury and A. C. Salisbury, pp. 757–773, Gulf Publishing Company, Houston, TX, 1996.
- Yang, X.-M., P. M. Davis, and J. H. Dieterich, Deformation from inflation of a dipping finite prolate spheroid in an elastic half-space as a model for volcanic stressing, *J. Geophys. Res.*, **93**, 4249–4257, 1988.

---

G. Anderson, S. Constable, H. Staudigel, and F. K. Wyatt, Institute of Geophysics and Planetary Physics, Scripps Institution of Oceanography, La Jolla, CA 92093-0225. (e-mail: anderson@python.ucsd.edu; sconstable@ucsd.edu; hstaudig@ucsd.edu; wyatt@ramsdn.ucsd.edu)

---

This preprint was prepared with AGU's L<sup>A</sup>T<sub>E</sub>X macros v5.01, with the extension package 'AGU++' by P. W. Daly, version 1.6b from 1999/08/19.